

Analytical and experimental study on natural sloshing frequencies in annular cylindrical tank with a bottom gap

H.W. Lee¹, S.H. Jeon¹, J.R. Cho², M.W. Seo¹ and W.B. Jeong^{*1}

¹School of Mechanical Engineering, Pusan National University, Busan 609-735, Korea

²Department of Naval Architecture and Ocean Engineering, Hongik University, Sejong 339-701, Korea

(Received April 1, 2015, Revised January 23, 2016, Accepted January 26, 2016)

Abstract. This paper is concerned with the analytical derivation of natural sloshing frequencies of liquid in annular cylindrical tank and its verification by experiment. The whole liquid domain is divided into three simple sub-regions, and the region-wise linearized velocity potentials are derived by the separation of variables. Two sets of matrix equations for solving the natural sloshing frequencies are derived by enforcing the boundary conditions and the continuity conditions at the interfaces between sub-regions. In addition, the natural sloshing frequencies are measured by experiment and the numerical accuracy of the proposed analytical method is verified through the comparison between the analytical and experimental results. It is confirmed that the present analytical method provides the fundamental sloshing frequencies which are in an excellent agreement with the experiment. As well, the effects of the tank radial gap, the bottom flow gap and the liquid fill height on the fundamental sloshing frequency are parametrically investigated.

Keywords: liquid sloshing; annular cylindrical tank; natural frequency; three flow regions; linearized velocity potential; analytical derivation; experimental verification

1. Introduction

Free surface fluctuation of liquid filled in various containers, called liquid sloshing, can be easily found all around us, such as a cup of coffee in hand, aboveground liquid storage tanks subject to earthquake wave, liquefied fuel in moving containers of automotive, vessel and aircraft (Baur 1966, Cho *et al.* 2001, Xue and Lin 2011, Moslemi *et al.* 2011, Lukovsky *et al.* 2012, Jia *et al.* 2015). Liquid sloshing may cause the structural failure of container and its main structural system, even further the tremendous loss of economic, environmental and human resources. But, on the other hand, it can be usefully used to suppress the vibration-induced structural dynamic instability (Yamamoto and Kawaha 1999, Banerji and Samanta 2011, Chakraborty *et al.* 2012, Love and Tait 2012). In offshore engineering, the study on the application of liquid sloshing to the control of structural dynamic stability for floating offshore wind turbine is intensively in progress (Tait *et al.* 2004, Lee *et al.* 2006, Colwell and Basu 2009). In these aspects, the investigation of sloshing phenomenon and its suppression and utilization have been a continuously challenging

*Corresponding author, Ph.D., E-mail: wbyeong@pusan.ac.kr

subject for many investigators during several decades (Ibrahim 2005).

In liquid-filled container, the structure deformation and the liquid pressure interact at the common liquid-structure interface, but its free vibration behavior is characterized by two quite distinct modes, sloshing and bulging modes (Veletsos and Yang 1976, Cho and Song 2001). In relatively lower frequency range, the liquid free-surface fluctuation (i.e., the sloshing mode) dominates, while the structure deformation becomes prevail as the natural frequency goes higher (i.e., the bulging mode). Furthermore, it has been reported that only a certain amount of liquid in the upper liquid region takes part in the free surface motion, while the rest of liquid contributes to the structure bulging mode as an added mass (Cho and Song 2001, Tedesco *et al.* 1987). The coupling between the liquid sloshing mode and the structure bulging mode becomes diminishes as the thickness (i.e., the stiffness) of container increases. In addition, due to the partial participation of liquid, the natural sloshing frequencies are significantly influenced by the liquid fill height (Cho *et al.* 2002) as well as the geometry and dimension of container.

The suppression of liquid sloshing could be made by altering the flow direction or by weakening the flow velocity, and a number of devices have been introduced for this purpose (Amabili *et al.* 1998, Xue and Lin 2011). Among them, baffles are widely used thanks to their easy installation and the high suppression performance. Baffles installed within the container characterize a whole flow region into several sub-regions of flows (not completely separated), so that the alteration of flow direction in the vicinity of baffles weakens the sloshing amplitude (Cho and Lee 2003, 2004, Akyildiz 2012, Koh *et al.* 2013). Contrary to the sloshing suppression devices, liquid motion in the container may transform the external vibration energy delivered to the container into the flow potential energy according to the free surface fluctuation. And, such vibration absorption efficiency can be maximized when the sloshing frequency approaches to the excitation frequency (Yamamoto and Kawahara 1999, Cho *et al.* 2005). Tuned liquid damper (TLD) and tuned liquid column damper (TLCD) which are widely used nowadays for the seismic design of high-rise buildings were motivated by the vibration energy absorption characteristic of liquid sloshing (Kim and Adeli 2005, Bhargava *et al.* 2005, Banerji and Samanta 2011, Chakraborty *et al.* 2012).

Meanwhile, floating offshore wind turbines, particularly those supported by spar-type platform, are subject to wave, current and wind excitations of the high irregularity in the frequency and direction. In addition, pitch and roll motions of floating offshore wind turbine are characterized by relatively low frequencies, and furthermore the total mass of liquid damper to be installed should be as small as possible in order not to alter the inherent dynamic characteristic of wind turbine. The center of mass of floating wind turbine is desired to be positioned at below to maximize the structural dynamic stability, but the relatively heavy liquid damper may move the center of mass upwards. Considering these distinguished aspects of floating offshore wind turbine compared to aboveground high-rise building, a shallow lightweight cylindrical TLD would be attractable for floating offshore wind turbine.

Cylindrical TLDs are classified into shallow and deep types based on the relative liquid fill height to the container characteristic length, and the limit of the relative liquid fill height for shallow TLD is around 10~12% according to Dean and Dalrymple (1984). It has been known that shallow TLDs provide the high sloshing damping thanks to the wave breaking phenomenon. However, Morsy (2010) reported that shallow TLD is not practical owing to the extreme nonlinearity stemming from the large free surface fluctuation and the occurrence of unpredictable wave breaking. Owing to the highly nonlinear liquid sloshing including the wave breaking phenomenon, the tuning of sloshing frequency of shallow cylindrical TLD becomes difficult.

Owing to this problem of shallow cylindrical TLD, an annular cylindrical tank is attractive for suppressing the structural vibration of floating offshore wind turbine subject to multi-directional irregular wave, current and wind excitations. It is because the weight of annular cylindrical tank is relatively smaller than non-annular one for the same liquid fill height and thence the desired damping performance could be obtained with the reasonable liquid fill height without causing the wave breaking phenomenon.

As an extension of our previous work on the analytical derivation of natural sloshing frequencies of liquid in cylindrical tank considering the flow compressibility (Cho *et al.* 2002), this paper addresses the analytical derivation of natural sloshing frequencies of liquid in annular cylindrical tank and the verification by experiment. Based upon the assumption of small-amplitude ideal sloshing flow, the flow potential is decomposed into three for three sub-regions of liquid according to the linearity of the Laplace equation. Sub-region-wise velocity potentials are analytically derived by the separation of variables and the matrix equations for solving the natural sloshing frequencies are obtained by applying the flow boundary conditions and the continuity conditions at the common interfaces between sub-regions of liquid. The sloshing experiments are also carried out to verify the numerical accuracy of the proposed analytical method. In addition, the fundamental sloshing frequency is parametrically investigated by the analytical and experimental methods with respect to the tank radial gap, the bottom flow gap and the liquid fill height.

2. Analytic derivation of natural sloshing frequencies

2.1 Liquid sloshing in annular cylindrical tank

Fig. 1 shows a three-dimensional annular cylindrical tank in which liquid is filled up to the height $h_w=h_1+h_2$ from the tank bottom in the stationary condition. Tank is assumed to be rigid and h_w and h_2 indicate the liquid fill height and the bottom flow gap respectively. The reader may refer to (Tedesco *et al.* 1987, Cho *et al.* 2002) for the flexible baffled tank (Veletsos and Yang 1976, Amabili *et al.* 1998) and the structure flexibility effect on the liquid sloshing. A cylindrical co-ordinate system with the z -axis being the tank axis is originated at point O . Even though the baffle thickness is neglected, the boundary of the liquid domain $\Omega \in \mathbb{R}^3$ is composed of the liquid-structure interface $\partial\Omega_l$ and the free surface $\partial\Omega_f$, as depicted in Fig. 1.

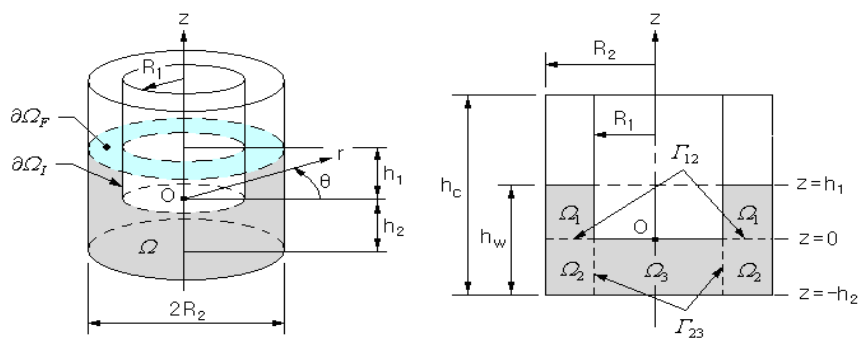


Fig. 1 Liquid sloshing in 3-D annular cylindrical tank

Assuming that the interior liquid flow $\mathbf{v}(\mathbf{x},t)$ is inviscid, incompressible and irrotational so that there exists a velocity potential function $\varphi(\mathbf{x},t): \mathbf{v}=\nabla\varphi$, the interior potential flow is governed by

$$\nabla^2\varphi = \frac{1}{r}\frac{\partial}{\partial r}\left(r\frac{\partial\varphi}{\partial r}\right) + \frac{1}{r^2}\frac{\partial^2\varphi}{\partial\theta^2} + \frac{\partial^2\varphi}{\partial z^2} = 0, \quad \text{in } \Omega \quad (1)$$

with the boundary condition at the structure-liquid interface

$$\nabla\varphi \cdot \mathbf{n} = 0, \quad \text{on } \partial\Omega_I \quad (2)$$

and the linearized dynamic and kinematic conditions on the free surface

$$\frac{\partial\varphi}{\partial t} + g\zeta = 0 \quad \text{and} \quad \frac{\partial\varphi}{\partial z} = \frac{\partial\zeta}{\partial t}, \quad \text{on } \partial\Omega_F \quad (3)$$

Here, \mathbf{n} denotes the outward unit vector normal to the liquid boundary and ζ is the free-surface elevation height, respectively. The dynamic and kinematic conditions in Eq. (3) can be combined into a unified linearized free surface condition given by (Cho *et al.* 2005)

$$\frac{\partial^2\varphi}{\partial t^2} + g\frac{\partial\varphi}{\partial z} = 0, \quad \text{on } \partial\Omega_F \quad (4)$$

For harmonically oscillating motion $\varphi(r, \theta, z; t) = \phi(r, \theta, z)e^{j\omega t}$, the unified linearized free surface condition ends up with

$$\frac{\partial\phi}{\partial z} = \lambda\phi, \quad \text{on } \partial\Omega_F \quad (5)$$

with λ being $\lambda = \omega^2 / g$. The liquid region Ω is divided into three sub-regions such that $\Omega = \Omega_1 \cup \Omega_2 \cup \Omega_3$ and the velocity potential ϕ is decomposed of

$$\phi = \phi_1 + \phi_2 + \phi_3 \quad (6)$$

according to the superposition principle. Then, three velocity potentials ϕ_I ($I=1, 2, 3$) defined in sub-regions Ω_I ($I=1, 2, 3$) should satisfy Eqs. (1) and (2) from the linearity of the Laplace operator, and the free surface condition given in Eq. (5) is additionally specified to ϕ_3 . In addition, each two adjacent velocity potentials should satisfy the flow continuity conditions at the common interfaces Γ_{12} at $z=0$ and Γ_{23} at $r=R_1$

$$\phi_1(r, \theta, 0) = \phi_2(r, \theta, 0) \quad \text{and} \quad \frac{\partial\phi_1}{\partial z} = \frac{\partial\phi_2}{\partial z}, \quad \text{at } \Gamma_{12} \quad (7)$$

$$\phi_2(R_1, \theta, z) = \phi_3(R_1, \theta, z) \quad \text{and} \quad \frac{\partial\phi_2}{\partial r} = \frac{\partial\phi_3}{\partial r}, \quad \text{at } \Gamma_{23} \quad (8)$$

In summary, the velocity potentials ϕ_I defined in sub-regions Ω_I should satisfy the Laplace equation, boundary conditions at the liquid-structure interfaces and free surface and the flow continuity conditions at the common interfaces.

2.2 Natural sloshing frequencies

In this section, the sub-region-wise velocity potential functions ϕ_I ($I=1,2,3$) for the harmonic sloshing motion are obtained by the separation of variables, and then a numerical formula for calculating the natural sloshing frequencies is derived. First, we let $\phi_1(r, \theta, z) = R_1(r) \cdot \Theta_1(\theta) \cdot Z_1(z)$ for the sub-region Ω_1 , then the above Laplace equation (1) for ϕ_1 is rewritten as

$$\frac{1}{r} \frac{d}{dr} \left(r \frac{dR_1(r)}{dr} \right) \frac{1}{R_1(r)} + \frac{1}{r^2} \frac{\Theta_1''(\theta)}{\Theta_1(\theta)} + \frac{\ddot{Z}_1(z)}{Z_1(z)} = 0 \tag{9}$$

where Θ_1'' and \ddot{Z}_1 indicate $d^2\Theta_1/d\theta^2$ and d^2Z_1/dz^2 , respectively. By letting $\Theta_1''/\Theta_1 = -m^2$ and $\ddot{Z}_1/Z_1 = k_1^2$, Eq. (9) becomes Bessel's differential equation of order m (Greenberg 1987)

$$r^2 \frac{d^2 R_1(r)}{dr^2} + r \frac{dR_1(r)}{dr} + ((k_1 r)^2 - m^2) R_1(r) = 0 \tag{10}$$

for $R_1(r)$. And, the general solution of Eq. (10) becomes

$$R_1(r) = A_1 J_m(k_1 r) + B_1 Y_m(k_1 r) \tag{11}$$

with the first- and second-kind Bessel functions $J_m(k_1 r)$ and $Y_m(k_1 r)$. Meanwhile, the general solutions for $\Theta_1(\theta)$ and $Z_1(z)$ are expressed by

$$\Theta_1(\theta) = a_3 \cos(m\theta) + a_4 \sin(m\theta) \tag{12}$$

$$Z_1(z) = a_5 \cosh(k_1 z) + a_6 \sinh(k_1 z) \tag{13}$$

Substituting the unified linearized free surface condition (5) into Eq. (13) leads to

$$a_6 = \frac{k_1 \sinh(k_1 h_1) - \lambda \cosh(k_1 h_1)}{\lambda \sinh(k_1 h_1) - k_1 \cosh(k_1 h_1)} a_5 \tag{14}$$

$$Z_1(z) = a_5 \left[\cosh(k_1 z) + \frac{k_1 \sinh(k_1 h_1) - \lambda \cosh(k_1 h_1)}{\lambda \sinh(k_1 h_1) - k_1 \cosh(k_1 h_1)} \sinh(k_1 z) \right] \tag{15}$$

and the velocity potential function $\phi_1(r, \theta, z)$ ends up with

$$\phi_1(r, \theta, z) = [a_1 J_m(k_1 r) + a_2 Y_m(k_1 r)] \left[\cosh(k_1 z) + \frac{k_1 \sinh(k_1 h_1) - \lambda \cosh(k_1 h_1)}{\lambda \sinh(k_1 h_1) - k_1 \cosh(k_1 h_1)} \sinh(k_1 z) \right] \Theta_1(\theta) \tag{16}$$

Here, the boundary conditions (2) at the liquid-structure interfaces at $r=R_1$ and $r=R_2$ provide us

$$[H_m(k_1)] \begin{Bmatrix} A_1 \\ B_1 \end{Bmatrix} = \begin{Bmatrix} 0 \\ 0 \end{Bmatrix}, \quad [H_m(k_1)] = \begin{bmatrix} J'_m(k_1 R_1) & Y'_m(k_1 R_1) \\ J'_m(k_1 R_2) & Y'_m(k_1 R_2) \end{bmatrix} \tag{17}$$

in which J'_m and Y'_m indicate the derivatives of Bessel functions with respect to r . Then, the separation variable k_1 which is used to calculate the natural sloshing frequencies is determined by

solving $\det([H_m(k_1)])=0$ with MATLAB.

In the similar manner, the potential function ϕ_2 in the sub-region Ω_2 is separated as $\phi_2(r, \theta, z) = R_2(r) \cdot \Theta_2(\theta) \cdot Z_2(z)$ with

$$R_2(r) = A_2 J_m(k_2 r) + B_2 Y_m(k_2 r) \quad (18)$$

$$Z_2(z) = b_5 \cosh(k_2 z) + b_6 \sinh(k_2 z) \quad (19)$$

Substituting the boundary condition (2) at $z = -h_2$ into Eq. (19) leads to

$$b_6 = \tanh(k_2 h_2) b_5 \quad (20)$$

and the resulting velocity potential ϕ_2 becomes

$$\phi_2(r, \theta, z) = [b_1 J_m(k_2 r) + b_2 Y_m(k_2 r)] \{ \cosh h(k_2 z) + \tanh(k_2 z) \sinh(k_2 z) \} \Theta_2(\theta) \quad (21)$$

The flow continuity conditions in Eq. (7) between ϕ_1 and ϕ_2 at the common interface Γ_{12} lead to

$$\lambda(k_1, k_2) = \frac{k_1^2 \tanh(k_1 h_1) + k_1 k_2 \tanh(k_2 h_2)}{k_2 \tanh(k_1 h_1) \tanh(k_2 h_2) + k_1} \quad (22)$$

and thus the natural sloshing frequencies defined in Eq. (5) are to be calculated by

$$\omega_n = \sqrt{g \lambda(k_1, k_2)}, \quad n = 1, 2, 3, \dots \quad (23)$$

Here, k_2 is to be determined by the boundary condition for h_2 at $r = R_2$ and the flow continuity conditions in Eq. (8) between ϕ_2 and ϕ_3 at the common interface Γ_{23} .

For the sub-region Ω_3 , we assume the liquid flow to be 2-D planar in order to let $\phi_3(r, \theta) = R_3(r) \cdot \Theta_3(\theta)$. Then, substituting ϕ_3 into Eq. (9), together with the separation of variables, leads to Euler-Cauchy equation given by

$$r^2 \frac{d^2 R_3(r)}{dr^2} + r \frac{dR_3(r)}{dr} - m^2 R_3(r) = 0 \quad (24)$$

and

$$\Theta_3''(\theta) + m^2 \Theta_3(\theta) = 0 \quad (25)$$

And, the general solution of ϕ_3 is expressed by

$$\phi_3(r, \theta) = (c_1 r^{-m} + c_2 r^m) \Theta_3(\theta) \quad (26)$$

in which c_1 should vanish in order not to allow $\phi_3 \rightarrow \infty$ at $r=0$ $r=0$. The boundary condition (2) of ϕ_3 at $r=R_2$ and the continuity conditions in Eq. (8) at the common interface Γ_{23} provide us

$$[H_m(k_2)] \begin{Bmatrix} b_1 \\ b_2 \\ c_1 \end{Bmatrix} = \begin{Bmatrix} 0 \\ 0 \\ 0 \end{Bmatrix}, \quad [H_m(k_2)] = \begin{bmatrix} J'_m(k_2 R_2) & Y'_m(k_2 R_2) & 0 \\ J'_m(k_2 R_1) & Y'_m(k_2 R_1) & -m R_1^{m-1} / k_2 \\ J_m(k_2 R_1) & Y_m(k_2 R_1) & -R_1^m \end{bmatrix} \quad (27)$$

Then, the separation variable k_2 which is required to determine $\lambda(k_1, k_2)$ in Eq. (22) is to be

calculated by solving $\det([H_m(k_2)])=0$ with MATLAB, as in the previous case for solving k_1 .

Two velocity potentials ϕ_2 and ϕ_3 are not continuous at all the points in the axial direction because the velocity potential ϕ_3 is assumed to be independent of z . In other words, the interface conditions in Eq. (8) can be satisfied only at a certain value between $z=0$ and $z=-h_2$ at the common interface Γ_{23} , which may be expected to be a source of discrepancy between the analytical and experimental results. Note that the axial position at $z=0$ is chosen to impose the continuity conditions for the current study.

3. Model cases and experiment setup

Fig. 2(a) shows a CAD model of annular cylindrical tank and the major geometry dimensions are represented in Fig. 2(b). The container is manufactured with acryl for clear visualization of the free surface fluctuation of liquid and water mixed with black dyes is used as liquid. The inner and outer cylinders are manufactured separately and then assembled by screwing two plates of the inner and outer cylinders. Four spacers having the equal size are inserted between two plates so that the bottom flow gap h_2 is adjusted by the thickness of spacers. Fig. 2(c) shows an acryl prototype of annular cylindrical tank, and three prototypes with the same outer radius of $R_2=170$ mm are manufactured for three different inner radii of $R_1=80,100$ and 120 mm. The height h_c of acryl container is 300 mm for all three tank models, but the bottom flow gap h_2 and the liquid fill height h_w are taken variable. Water is supplied into the annular cylindrical tank through the holes of two upper plates of inner and outer cylinders, and the tank thickness is thick enough such that its flexibility does not influence the sloshing frequency of interior liquid.

In order for the parametric investigation of fundamental sloshing frequencies, three bottom gaps and five liquid fill heights are considered for all three tank models, $h_2=10,20$ and 30 mm and $h_w=110, 120, 130, 140$ and 150 mm respectively. Thus, the total number of experiment cases are forty five, and each experiment case is repeatedly conducted by eight times to secure the reliability of experimental data. In accordance with the experiment, the fundamental sloshing frequencies are

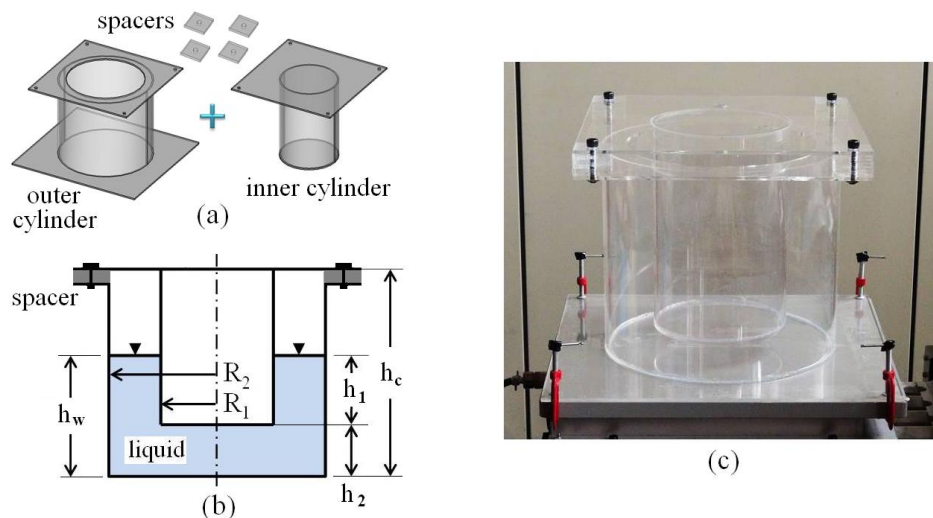


Fig. 2 Annular cylindrical tank: (a) CAD model, (b) geometry dimensions, (c) acryl prototype

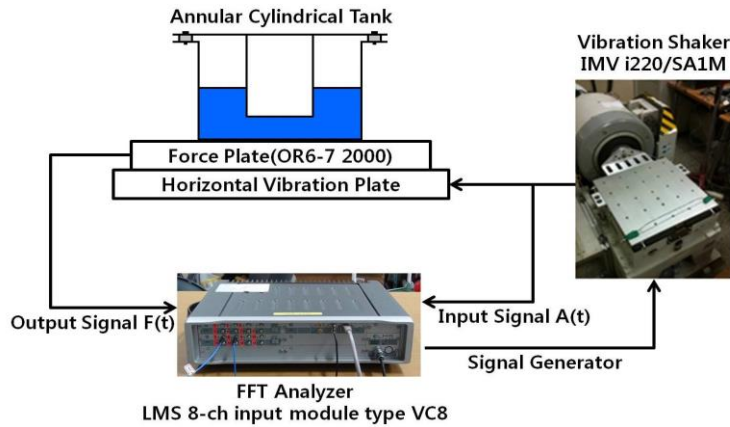


Fig. 3 Configuration of excitation and data acquisition system

Table 1 Setting of FFT analyzer

Span	Lines	Resolution	Overlap	Average
12.5 Hz	800	0.015625 Hz	75%	20

Table 2 Specifications of the other equipments

Accelerometer (Kistler 8310B10)	Acceleration range	Sensitivity, 5%	Resolution (threshold)	Frequency Response, 5%	Noise type (0 ~ 100 Hz)
	10 g	197 mV/g	2,830 μg	0~180 Hz	2,000 μg_{rms}
Force plate (OR6-7 2000)	Capacity	Sensitivity	Excitation	Hysteresis	Natural frequency
	4,450 N	0.34 mV/N	max 10V	0.2%	370 Hz
Exciter (i220/SA1M)	Frequency range		Maximum acceleration and payload		
	DC~2,500 Hz		203 m/s ² , 200 kg		

also analytically calculated by solving Eqs. (17), (22) and (27) and compared with experimental data. Fig. 3 represents an excitation and data signal acquisition system composed of signal generator, vibration shaker, FFT analyzer, horizontal vibration plate and force plate, where a random white noise signal ranging 0~25 Hz, which is generated by the digital signal generator, is delivered to the vibration shaker to excite the horizontal vibration table. A strain gage-type force plate is installed between the horizontal vibration table and a partially filled annular cylindrical tank in order to measure the sloshing-induced force which is transmitted from the annular cylindrical tank to the horizontal vibration plate. The major specifications of each component in the system are given in Tables 1 and 2.

Fig. 4 shows a real scene of sloshing experiment, where an accelerometer is attached between the horizontal vibration plate and the vibration shaker to measure the force plate acceleration (i.e., the input signal). Meanwhile, the force plate measures the transmission force exerted on the horizontal vibration plate which is caused by interior liquid sloshing in the annular cylindrical tank. Then, the apparent mass $H(\omega)$, a kind of frequency response function (FRF), is defined by the relative output (the force F_{vp} exerted on the vibration plate) with respect to the input (the acceleration a_{vp} of the vibration plate):

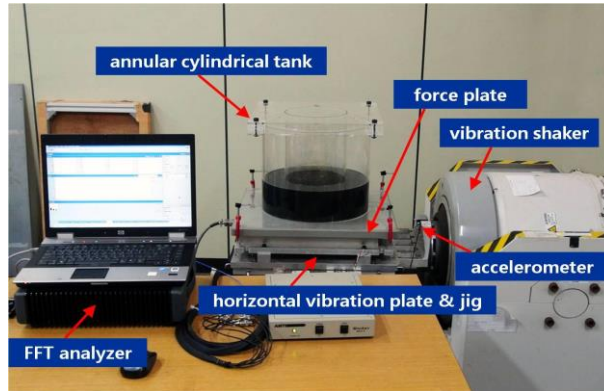


Fig. 4 Scene of sloshing experiment

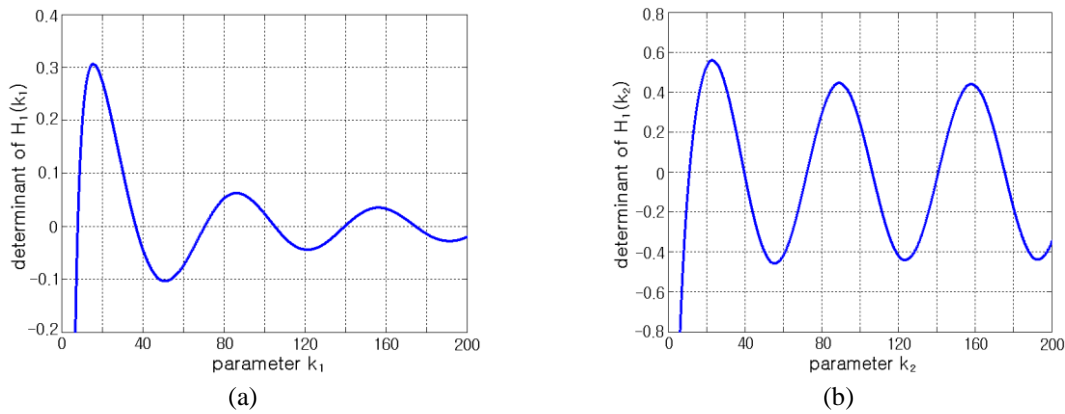


Fig. 5 (a) Determinant of $H_1(k_1)$, (b) determinant of $H_1(k_2)$

$$H(\omega) = \frac{\text{force exerted on the vibration plate}}{\text{accelerati on of the vibrationplate}} = \frac{F_{vp}}{a_{vp}} \quad (28)$$

The detailed analytical derivation of the apparent mass $H(\omega)$ of the partially filled annular cylindrical tank on the horizontal vibration plate is given in Appendix.

4. Comparison of analytical and experimental results

In order to analytically calculate the fundamental sloshing frequencies ω_n defined in Eq. (23), we first should determine k_1 and k_2 from the determinants of $H_m(k_1)$ and $H_m(k_2)$. But, since these two determinants are in function of R_1, R_2, m as well as k_1 and k_2 , as given in Eqs. (17) and (27), one should plot the determinants of $H_m(k_1)$ and $H_m(k_2)$ with respect to k_1 and k_2 for given values of R_1, R_2 and m . Note that two determinants $H_m(k_1)$ and $H_m(k_2)$ are independent of the bottom flow gap h_2 and the liquid fill height h_v , so that two plots are needed only for three different tank models. In the current study, the first and second Bessel functions of order 1 (i.e., $m=1$) are taken to calculate two determinants.

Figs. 5(a) and 5(b) represent the plots of determinants of $H_1(k_1)$ and $H_1(k_2)$ for tank model I with $R_1=80$ mm and $R_2=170$ mm, from where we choose the lowest k_1 and k_2 which make the determinants of $H_m(k_1)$ and $H_m(k_2)$ be zero. All the values of k_1 and k_2 for three tank models are determined in this manner, and then natural sloshing frequencies for forty five cases with different bottom flow gap h_2 and the liquid fill height h_w are calculated using Eqs. (22) and (23). The analytically calculated fundamental sloshing frequencies are given in Tables 3, 4 and 5, where the analytical results are arranged and compared with experimental data for each tank model.

Next, the experiments were performed for forty five cases to examine the frequency responses of apparent mass of partially filled annular cylindrical tank. Each frequency response was measured by exciting the tank with white noise with the frequency range of 0~20 Hz, and lowest natural sloshing frequencies and mode shapes were sought by the resonance frequencies of apparent mass. Fig. 6 shows the first and second sloshing mode shapes for tank model I with $R_1=80$ mm, $R_2=170$ mm, $h_2=10$ and $h_w=110$ mm. The first sloshing mode shows a seesaw-like free surface fluctuation, while the second one shows a full sine wave-like free surface motion such that water on the left moves up while one on the right moves down. However, the current study focuses on the fundamental sloshing frequency because it characterizes the structural vibration of partially filled liquid tank.

Fig. 7 shows the frequency responses of fundamental apparent mass $H(\omega)$ of tank model I having the largest radial gap (R_2-R_1) of 90 mm with respect to the liquid fill height h_w for three different bottom flow gap h_2 . First of all, it is observed that the fundamental resonance frequency and the apparent mass uniformly increases in proportional to the liquid fill height regardless of the bottom flow gap. And, in proportional to the bottom flow gap, the increase of the fundamental

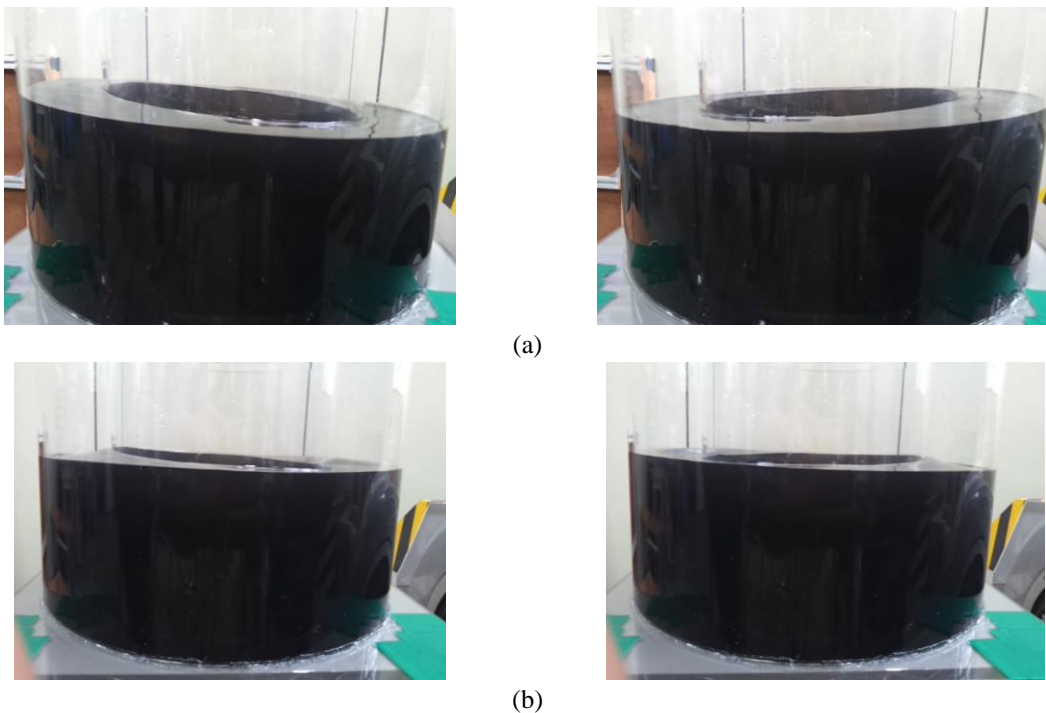


Fig. 6 Sloshing mode shapes: (a) first, (b) second

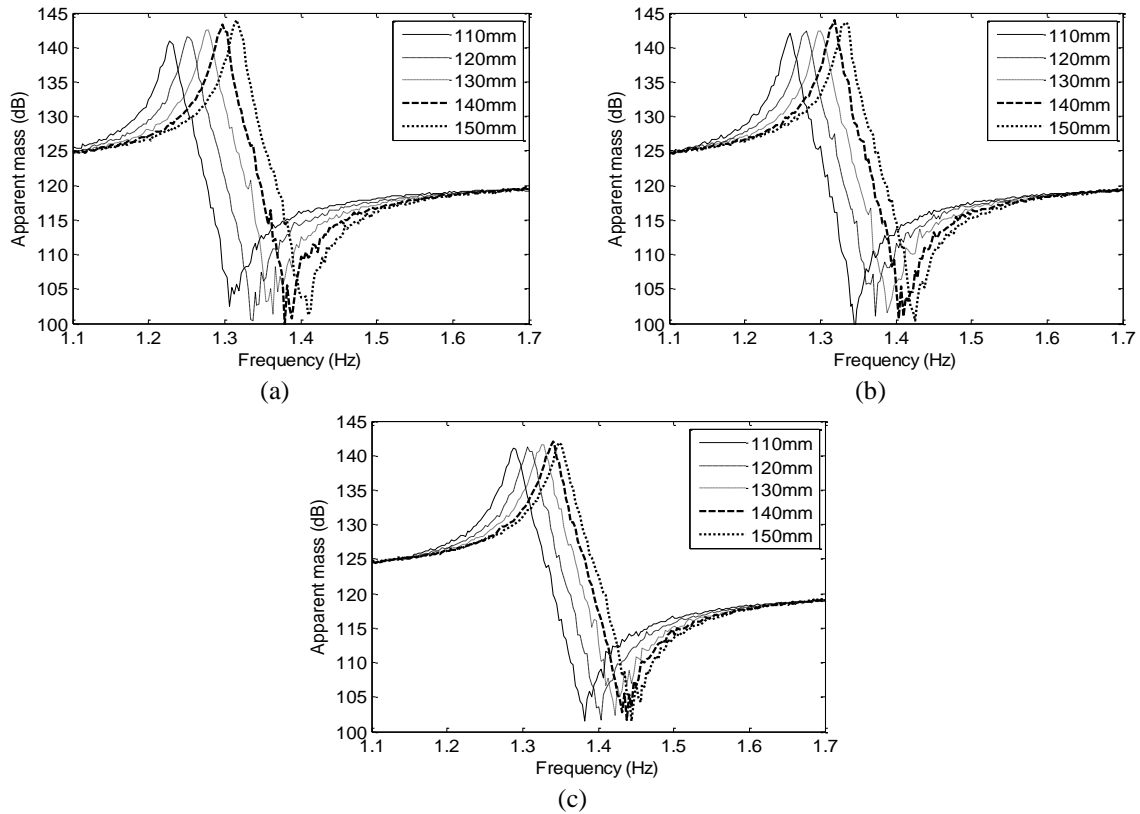


Fig. 7 Frequency responses of the fundamental apparent mass $H(\omega)$ to the liquid fill height h_w for tank model I: (a) $h_2=10$ mm, (b) $h_2=20$ mm, (c) $h_2=30$ mm

resonance frequency is apparent while the change of apparent mass is not remarkable. But, the influence of liquid fill height on the variance of resonance frequency and the magnitude of apparent mass is shown to be smaller as the bottom flow gap becomes larger. Thus, it can be inferred from this trend that the bottom flow gap counteracts with the influence of liquid fill height on the fundamental resonance frequency and the apparent mass. Referring to Fig. 2(b), for a given liquid fill height h_w , the net vertical flow height h_1 becomes smaller as the bottom flow gap h_2 increases, which gives rise to a counteracting effect on the parametric trend of fundamental sloshing frequency and apparent mass to the liquid fill height. In other words, the relative horizontal flow amount at the bottom increases in proportional to the bottom flow gap h_2 , when compared with the vertical flow amount, which weakens the influence of liquid fill height on the variation of fundamental sloshing frequency and apparent mass.

The frequency responses of apparent mass of tank model III with the inner radius R_1 of 120 mm, a tank model having the smallest radial gap (R_2-R_1) equal to 50 mm. As in the previous tank model I, the fundamental resonance frequency uniformly increases in proportional to the liquid fill height h_w , even though the increase of apparent mass is not remarkable, regardless of the bottom flow gap h_2 . And, in proportional to the bottom flow gap, the increase of the fundamental resonance frequency becomes apparent and the influence on the variance of fundamental resonance frequency becomes smaller. But, when compared with the previous tank model I, the

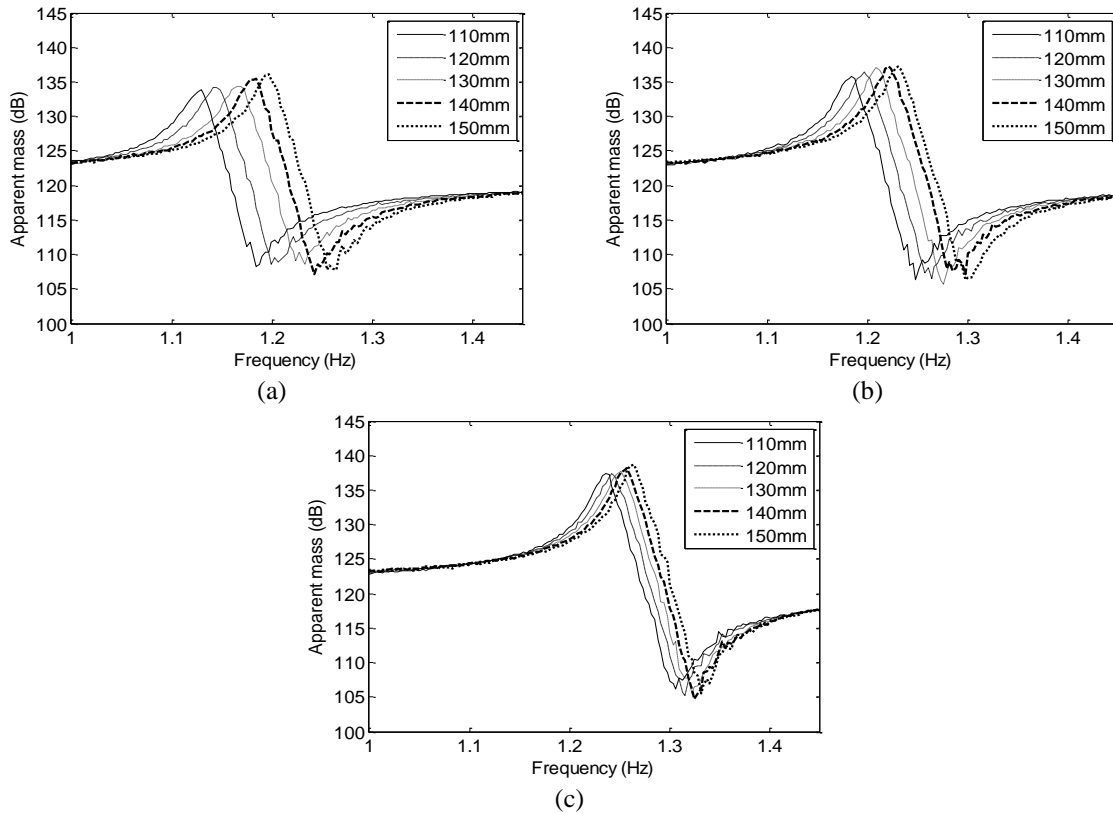


Fig. 8 Frequency responses of the fundamental apparent mass $H(\omega)$ to the liquid fill height h_w for tank model III: (a) $h_2=10$ mm, (b) $h_2=20$ mm, (c) $h_2=30$ mm

fundamental sloshing frequencies are lower and their variance to the liquid fill height is smaller for all three bottom flow gaps. In addition, it is observed that the apparent masses are smaller and slightly increase in proportional to the bottom flow gap. Thus, it is found that the fundamental sloshing frequency, its variation to the liquid fill height and the apparent mass become smaller as the gap between inner and outer cylinders decreases. But, the apparent mass slightly increases with h_2 as the tank radial gap decreases. The liquid sloshing frequency in cylindrical tank increases in proportional to the total liquid volume and inversely proportional to the area of liquid free surface (Cho and Song 2001), and the apparent mass increases with the total liquid mass. Thus, the above-mentioned trend with respect to the radial gap of the annular tank is consistent with the fact that the total liquid mass decreases inversely proportional to the radial gap ($R_2 - R_1$) and in proportional to the bottom flow gap h_2 , for given outer radius R_2 of tank and the liquid fill height. As well, the decrease of liquid free surface is relatively smaller than the decrease of the total liquid volume, for a given decrease in the radial gap.

The fundamental sloshing frequencies measured by experiments are recorded in Tables 3, 4 and 5 for tank models I, II and III respectively, where the errors indicate the relative differences of theoretical values with respect to the experimental data. It is observed from the detailed numerical values that the maximum relative error is 0.685% for all forty five cases, which clearly verifies the reliability of the analytical method introduced in the current study. The largest relative error occurs

Table 3 Fundamental sloshing frequencies (Hz) for tank model I to the liquid fill height h_w

Dimensions of liquid tank (mm)				Method	Liquid fill height h_w (mm)				
R_1	R_2	(R_2-R_1)	h_2		110	120	130	140	150
80	170	90	10	Theory	1.2307	1.2580	1.2816	1.3020	1.3195
				Experiment	1.2268	1.2512	1.2787	1.2970	1.3153
				Error (%)	0.318	0.543	0.227	0.386	0.319
			20	Theory	1.2569	1.2806	1.3011	1.3187	1.3339
				Experiment	1.2604	1.2817	1.3000	1.3184	1.3336
				Error (%)	-0.278	-0.086	0.085	0.023	0.022
			30	Theory	1.2818	1.3022	1.3196	1.3346	1.3475
				Experiment	1.2878	1.3062	1.3245	1.3397	1.3489
				Error (%)	-0.466	-0.306	-0.370	-0.381	-0.104

*Error indicates the relative difference with respect to experiment.

Table 4 Fundamental sloshing frequencies (Hz) for tank model II to the liquid fill height h_w

Dimensions of liquid tank (mm)				Method	Liquid fill height h_w (mm)				
R_1	R_2	(R_2-R_1)	h_2		110	120	130	140	150
100	170	70	10	Theory	1.1672	1.1930	1.2155	1.2352	1.2523
				Experiment	1.1627	1.1871	1.2085	1.2268	1.2451
				Error (%)	0.387	0.497	0.579	0.685	0.578
			20	Theory	1.2073	1.2280	1.2461	1.2618	1.2754
				Experiment	1.2054	1.2238	1.2421	1.2573	1.2695
				Error (%)	0.158	0.343	0.322	0.358	0.465
			30	Theory	1.2441	1.2601	1.2740	1.2860	1.2965
				Experiment	1.2421	1.2573	1.2726	1.2848	1.2939
				Error (%)	0.161	0.223	0.110	0.093	0.201

Table 5 Fundamental sloshing frequencies (Hz) for tank model III to the liquid fill height h_w

Dimensions of liquid tank (mm)				Method	Liquid fill height h_w (mm)				
R_1	R_2	(R_2-R_1)	h_2		110	120	130	140	150
120	170	50	10	Theory	1.1246	1.1475	1.1678	1.1856	1.2014
				Experiment	1.1292	1.1444	1.1658	1.1841	1.1963
				Error (%)	-0.407	0.271	0.172	0.127	0.426
			20	Theory	1.1838	1.1998	1.2138	1.2261	1.2369
				Experiment	1.1841	1.1963	1.2085	1.2207	1.2299
				Error (%)	-0.025	0.293	0.439	0.442	0.569
			30	Theory	1.2356	1.2453	1.2537	1.2611	1.2676
				Experiment	1.2360	1.2421	1.2512	1.2573	1.2634
				Error (%)	-0.032	0.258	0.200	0.302	0.332

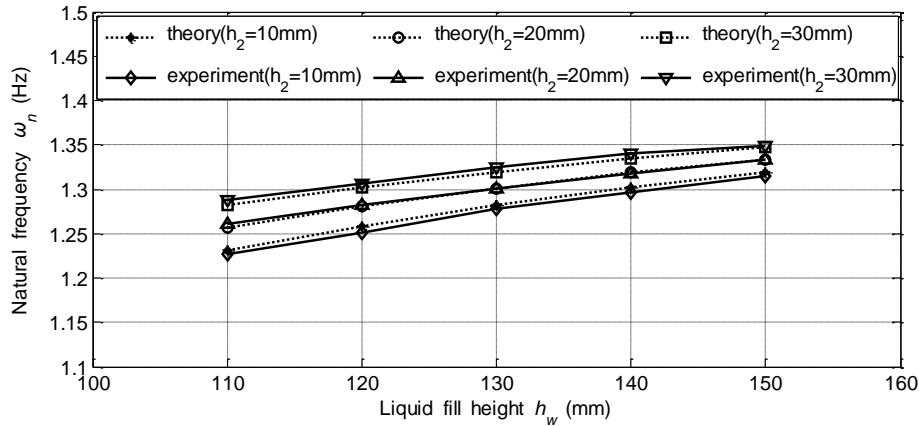


Fig. 9 Comparison of fundamental sloshing frequencies between theoretical and experimental methods for tank model I

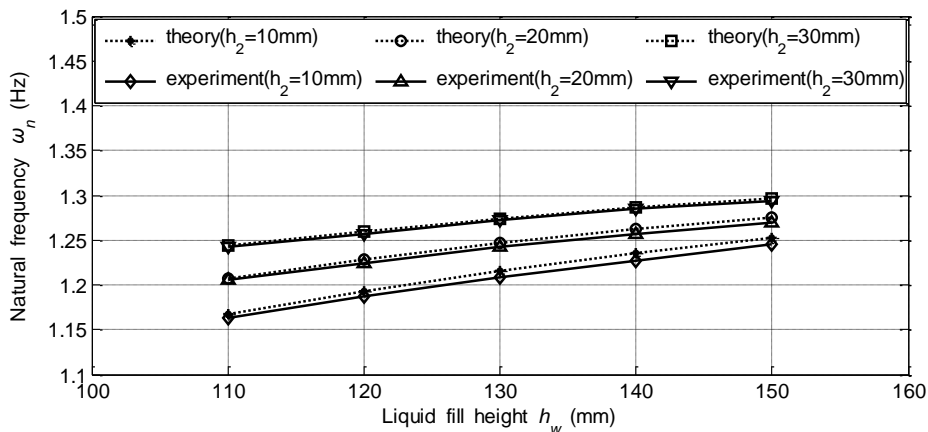


Fig. 10 Comparison of fundamental sloshing frequencies between theoretical and experimental methods for tank model II

at tank model II, while the peak relative errors at tank models I and III are 0.543% and 0.569% respectively. The occurrence of the largest relative error at tank model II is not owing to the consistency but a coincidence stemming from the inherent experimental error.

The parametric variation of fundamental sloshing frequencies and the comparison with the experiment are represented in Figs. 9-11 for tank models I, II and III, respectively. For all three tank models, the fundamental sloshing frequencies obtained by the analytical method and experiment show the uniform increase in proportional to the liquid fill height h_w and to the bottom flow gap h_2 . It is because the total liquid volume becomes larger as the liquid fill height and the bottom flow gap increase, for given inner and outer radii of annular cylindrical tank. It is also clearly observed that the increase of fundamental sloshing frequency with the liquid fill height becomes smaller as tank model changes from I to III, that is, as the radial gap ($R_2 - R_1$) becomes smaller. These parametric trends of fundamental sloshing frequencies have been observed from the previous frequency responses of apparent mass which are shown in Figs. 7 and 8. Here, it is

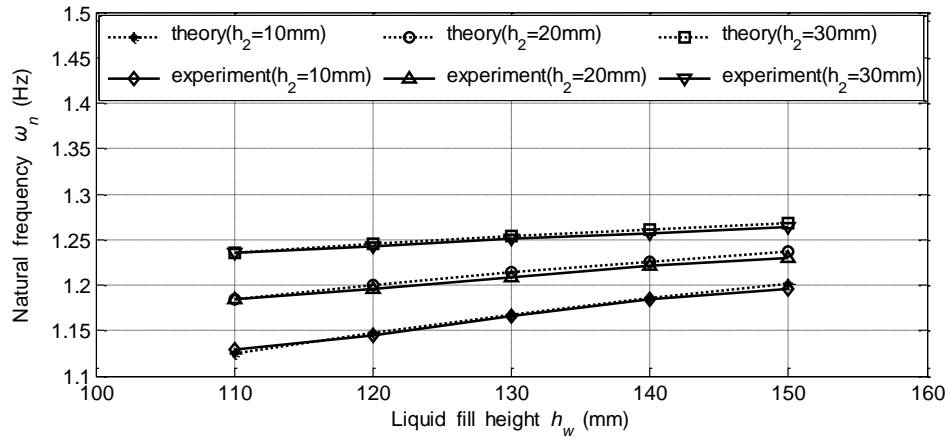


Fig. 11 Comparison of fundamental sloshing frequencies between theoretical and experimental methods for tank model III

observed that the variation of fundamental sloshing frequencies to the bottom flow gap h_2 becomes larger at lower liquid fill height, and which becomes apparent as the tank radial gap ($R_2 - R_1$) decreases. Referring to Fig. 2(b) showing the tank geometry, it is because the portion of liquid volume increase produced by increasing the bottom flow gap becomes more significant as either the liquid fill height or the tank radial gap decreases.

Meanwhile, it is observed that the analytical method as a whole provides the fundamental sloshing frequencies slightly higher than the experiment, except for a few cases at lower liquid fill heights and larger bottom flow gaps in tank model I and at the lowest liquid fill height in tank model III. Referring to Fig. 1 showing the three sub-regions of liquid flow, the flow regions Ω_2 and Ω_3 occupy a relatively remarkable portion in the total flow region at these few cases, so the flow continuity enforcement at $z=0$ between two flow regions is inferred to lead such theoretical values lower than the experimental data. Except for this singularity, there exist no apparent parametric trend in the relative errors with respect to the liquid fill height, the bottom flow gap and the tank radial gap. And, it is confirmed that the fundamental sloshing frequencies predicted by the proposed analytical method for partially filled annular cylindrical tanks are in excellent agreement with the experimental data with the maximum relative error less than 1.0%.

5. Conclusions

An analytical method for calculating the natural liquid sloshing frequencies in annular cylindrical tanks has been introduced, and its prediction accuracy has been verified through the comparison with the experiments. The flow region was divided into three sub-regions and the region-wise potential flows were analytically derived by the separation of variables, and then the numerical formula for calculating the natural liquid sloshing frequencies were derived by enforcing the flow continuity conditions at the common interfaces between sub-regions. Meanwhile, forty five experiment cases were conducted by changing three parameters, the tank radial gap, the bottom flow gap and the liquid fill height, and the frequency responses of apparent mass of partially filled annular cylindrical tanks were measured.

It has been verified from the comparison with the experiment that the proposed analytical method predicts the fundamental sloshing frequencies with the maximum relative error of 0.685%. In addition, from the parametric investigation of fundamental sloshing frequencies, the following main observations are found. First, the fundamental sloshing frequency and the apparent mass uniformly increase in proportional to the bottom flow gap and the liquid fill height, but the increase of fundamental sloshing frequency with the liquid fill height slows down as the tank radial gap becomes smaller. Second, the influence of liquid fill height on the variance of fundamental sloshing frequency slows down in proportional to the bottom flow gap, and this trend becomes more apparent as the tank radial gap decreases. And, the variation of fundamental sloshing frequencies to the bottom flow gap prevails at lower liquid fill height, and which becomes apparent as the tank radial gap decreases. Finally, the proposed analytical method as a whole predicts the fundamental sloshing frequencies slightly higher than the experimental, except for a few cases at lower liquid fill height and larger bottom flow gap.

Acknowledgements

This work was supported by the Human Resources Development of the Korea Institute of Energy Technology Evaluation and Planning (KETEP) grant funded by the Korea Ministry of Knowledge Economy (No. 20113020020010).

References

- Akyildiz, A. (2012), "A numerical study of the effects of the vertical baffle on liquid sloshing in two-dimensional rectangular tank", *J. Sound Vib.*, **331**(1), 41-52.
- Amabili, M., Païdousis, M.P. and Lakis, A.A. (1998), "Vibrations of partially filled cylindrical tanks with ring-stiffeners and flexible bottom", *J. Sound Vib.*, **213**(5), 259-299.
- Banerji, P. and Samanta, A. (2011), "Earthquake vibration control of structures using hybrid mass liquid damper", *Eng. Struct.*, **33**(4), 1291-1301.
- Baur, H.F. (1996), "Nonlinear mechanical model for the description of propellant sloshing", *AIAA J.*, **4**(9), 1662-1668.
- Bhargava, K., Ghosh, A.K. and Ramanujam, S. (2005), "Seismic response and failure modes for a water storage structure-A case study", *Struct. Eng. Mech.*, **20**(1), 1-20.
- Chakraborty, S., Debbarma, R. and Marano, G.C. (2012), "Performance of tuned liquid column dampers considering maximum liquid motion in seismic vibration control of structures", *J. Sound Vib.*, **331**(7), 1519-1531.
- Cho, J.R., Song, J.M. and Lee, J.K. (2001), "Finite element techniques for the free-vibration and seismic analysis of liquid-storage tanks", *Finite Elem. Anal. Des.*, **37**, 467-483.
- Cho, J.R. and Song, J.M. (2001), "Assessment of classical numerical models for the separate fluid-structure modal analysis", *J. Sound Vib.*, **239**(5), 995-1012.
- Cho, J.R., Kim, K.W., Lee, J.K., Park, T.H. and Lee, W.Y. (2002), "Axisymmetric modal analysis of liquid-storage tanks considering compressibility effects", *Int. J. Numer. Meth. Eng.*, **55**, 733-752.
- Cho, J.R., Lee, H.W. and Kim, K.W. (2002), "Free vibration analysis of baffled liquid-storage tanks by the structural-acoustic finite element formulation", *J. Sound Vib.*, **258**(5), 847-866.
- Cho, J.R. and Lee, S.Y. (2003), "Dynamic analysis of baffled fuel-storage tanks using the ALE finite element method", *Int. J. Numer. Meth. Fluid.*, **41**, 185-208.
- Cho, J.R. and Lee, H.W. (2004), "Numerical study on liquid sloshing in baffled tank by nonlinear finite

- element method”, *Comput. Meth. Appl. Mech. Eng.*, **193**, 2581-2598.
- Cho, J.R., Lee, H.W. and Ha, S.Y. (2005), “Finite element analysis of resonant sloshing response in 2-D baffled tank”, *J. Sound Vib.*, **288**, 829-845.
- Colwell, S. and Basu, B. (2009), “Tuned liquid column dampers in offshore wind turbines for structural control”, *Eng. Struct.*, **31**, 358-368.
- Dean, R.G. and Dalrymple, D. (1984), *Water Wave Mechanics for Engineers and Scientists*, 1st Edition, Prentice-Hall, New Jersey.
- Greenberg, M.D. (1987), *Foundations of Applied Mathematics*, Prentice-Hall, New Jersey.
- Ibrahim, R.A. (2005), *Liquid Sloshing Dynamics, Theory and Applications*, Cambridge University Press, New York.
- Jia, D., Agrawal, M., Wang, C., Shen, J. and Malachowski, J. (2015), “Fluid-structure interaction of liquid sloshing induced by vessel motion in floating LNG tank”, *ASME 2015 34th International Conference on Ocean, Offshore and Arctic Engineering*, OMAE2015-41463.
- Kim, H.J. and Adeli, A. (2005), “Hybrid control of irregular steel highrise building structures under seismic excitations”, *Int. J. Numer. Meth. Eng.*, **63**(12), 1757-1774.
- Koh, C.G., Luo, M., Gao, M. and Bai, W. (2013), “Modeling of liquid sloshing with constrained floating baffle”, *Comput. Struct.*, **122**, 270-279.
- Lee, H.H., Wong, S.H. and Lee, S.H. (2006), “Response mitigation on the offshore floating platform system with tuned liquid column damper”, *Ocean Eng.*, **33**, 1118-1142.
- Love, J.S. and Tait, M.J. (2012), “A preliminary design for tuned liquid dampers conforming to space restrictions”, *Eng. Struct.*, **40**, 187-197.
- Lukovsky, I., Ovchynnykov, D. and Timokha, A. (2012), “Asymptotic nonlinear multimodal modeling of liquid sloshing in an upright circular cylindrical tank. I. Modal equations”, *Nonlin. Oscillat.*, **14**(4), 512-525.
- Morsy, H. (2010), “A numerical study of the performance of tuned liquid dampers”, MD Thesis, McMaster University, Hamilton, Canada.
- Moslemi, M., Kianoush, M.R. and Pogorzelski, W. (2011), “Seismic response of liquid-filled elevated tanks”, *Eng. Struct.*, **33**(6), 2074-2084.
- Tait, M.J., Isyumov, N. and El Damatty, A.A. (2004), “The efficiency and robustness of a uni-directional tuned liquid damper and modeling with an equivalent TMD”, *Wind Struct.*, **7**(4), 235-250.
- Tedesco, J.W., Kostem, C.N. and Kalnins, A. (1987), “Free vibration of cylindrical liquid storage tanks”, *Comput. Struct.*, **26**(6), 957-964.
- Veletsos, A.S. and Yang, J.Y. (1976), “Dynamics of fixed-based liquid-storage tanks”, *Proceedings of US-Japan Seminar Earthquake Engineering Research*, 317-341.
- Xue, M.A. and Lin, P. (2011), “Numerical study of ring baffle effects on reducing violent liquid sloshing”, *Comput. Fluid.*, **52**, 116-129.
- Yamamoto, K. and Kawahara, M. (1999), “Structural oscillation control using tuned liquid damper”, *Comput. Struct.*, **71**, 435-446.

Appendix: Theoretical derivation of apparent mass $H(\omega)$

The sloshing experiment apparatus shown in Figs. 3 and 4, which is composed of a horizontal vibration plate and a partially filled annular cylindrical tank, can be modeled as a two-DOF mass-spring system, as represented in Fig. A1. Where, M_1 indicates the equivalent mass of the vibration plate, m_2 and k_3 denote the equivalent mass and stiffness of the annular cylindrical tank, respectively.

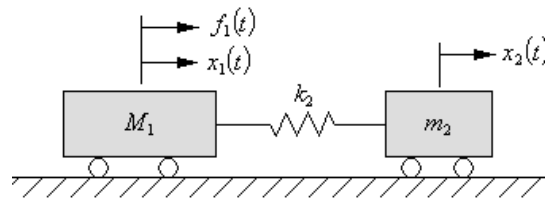


Fig. A1 A two-DOF dynamic model of the sloshing experiment apparatus

Letting $x_1(t)$ and $x_2(t)$ be the absolute horizontal dynamic motions of the vibration plate and the annular cylindrical tank and $f_1(t)$ be the excitation force, the equations of motion of the two-DOF dynamic model are expressed by

$$\begin{bmatrix} M_1 & 0 \\ 0 & m_2 \end{bmatrix} \begin{Bmatrix} \ddot{x}_1(t) \\ \ddot{x}_2(t) \end{Bmatrix} + \begin{bmatrix} k_2 & -k_2 \\ -k_2 & k_2 \end{bmatrix} \begin{Bmatrix} x_1(t) \\ x_2(t) \end{Bmatrix} = \begin{Bmatrix} f_1(t) \\ 0 \end{Bmatrix} \quad (\text{A1})$$

For harmonic excitation force $f_1(t) = Fe^{i\omega t}$, the resulting two absolute dynamic motions are expressed by $x_1(t) = A_1 e^{i\omega t}$ and $x_2(t) = A_2 e^{i\omega t}$. Substituting these harmonic responses into Eq. (A1) ends up with

$$\begin{bmatrix} M_1 - \frac{1}{\omega^2} k_2 & \frac{1}{\omega^2} k_2 \\ \frac{1}{\omega^2} k_2 & m_2 - \frac{1}{\omega^2} k_2 \end{bmatrix} \begin{Bmatrix} A_1 \\ A_2 \end{Bmatrix} = \begin{Bmatrix} F \\ 0 \end{Bmatrix} \quad (\text{A2})$$

Solving the simultaneous equations leads to the amplitude A_1 given by

$$A_1 = \frac{\left(m_2 - \frac{k_2}{\omega^2}\right) F}{\left(M_1 - \frac{k_2}{\omega^2}\right) \left(m_2 - \frac{k_2}{\omega^2}\right) - \frac{1}{\omega^4} k_2^2} \quad (\text{A3})$$

Finally, according to the definition given in Eq. (28), the apparent mass $H(\omega)$ of the annular cylindrical tank is calculated by

$$H(\omega) = \frac{F}{A_1} = \frac{(\omega^2 M_1 - k_2)(\omega^2 m_2 - k_2) - k_2^2}{\omega^2 (\omega^2 m_2 - k_2)} \quad (\text{A4})$$

Therefore, $H(\omega)$ has the peak value at the natural sloshing frequency of $\omega_r = \sqrt{k_2 / m_2}$ (rad/s) (or, $f_r = \omega_r / 2\pi$ (Hz)), whereas the anti-resonance of apparent mass occurs at the frequencies which make the numerator of Eq. (A4) be zero. It is found that both the resonance and anti-resonance of apparent mass are dependent of the equivalent mass and stiffness of the partially filled annular cylindrical tank as well as the equivalent mass of the vibration plate.